REPORT DOCUMENTATION PAGE

Form Approved OMB NO. 0704-0188

1. REPORT DATE (DD-MM-YYYY)	2. REPORT TYPE	3. DATES COVERED (From - To)
	New Reprint	-

4. TITLE AND SUBTITLE

An Atomically Layered InSe Avalanche Photodetector

5a. CONTRACT NUMBER	5b. GRANT NUMBER	5c. PROGRAM ELEMENT NUMBER	5d. PROJECT NUMBER	5e. TASK NUMBER	5f. WORK UNIT NUMBER
W911NF-11-1-0362		611103			

6. AUTHORS

Fangfang Wen, Liehui Ge, Sina Najmaei, Antony George, Yongji Gong, Weilu Gao, Zehua Jin, Bo Li, Jun Lou, Junichiro Kono, Robert Vajtai, Pulickel Ajayan, Naomi J. Halas, Sidong Lei

7. PERFORMING ORGANIZATION NAMES AND ADDRESSES

William Marsh Rice University
6100 Main Street

Houston, TX 77005 -1827

8. PERFORMING ORGANIZATION REPORT NUMBER

9. SPONSORING/MONITORING AGENCY NAME(S) AND ADDRESS (ES)

U.S. Army Research Office
P.O. Box 12211
Research Triangle Park, NC 27709-2211

10. SPONSOR/MONITOR'S ACRONYM(S)
ARO

11. SPONSOR/MONITOR'S REPORT NUMBER(S)
59735-MS-MUR.119

12. DISTRIBUTION AVAILIBILITY STATEMENT

Approved for public release; distribution is unlimited.

13. SUPPLEMENTARY NOTES

The views, opinions and/or findings contained in this report are those of the author(s) and should not contrued as an official Department of the Army position, policy or decision, unless so designated by other documentation.

14. ABSTRACT

Atomically thin photodetectors based on 2D materials have attracted great interest due to their potential as highly energy-efficient integrated devices. However, photoinduced carrier generation in these media is relatively poor due to low optical absorption, limiting device performance. Current methods for overcoming this problem, such as reducing contact resistances or back gating, tend to increase
dark current and suffer slow response times. Here, we realize the avalanche effect in a 2D material-based photodetector and show that avalanche multiplication can greatly enhance the device response of an ultrathin InSe

15. SUBJECT TERMS

InSe, 2D photodetector, avalanche effect, impact ionization

16. SECURITY CLASSIFICATION OF:			17. LIMITATION OF ABSTRACT	15. NUMBER OF PAGES	19a. NAME OF RESPONSIBLE PERSON
a. REPORT	b. ABSTRACT	c. THIS PAGE			Pullickel Ajayan
UU	UU	UU	UU		19b. TELEPHONE NUMBER 713-348-5904

Report Title

An Atomically Layered InSe Avalanche Photodetector

ABSTRACT

Atomically thin photodetectors based on 2D materials have attracted great interest due to their potential as highly energy-efficient integrated devices. However, photoinduced carrier generation in these media is relatively poor due to low optical absorption, limiting device performance. Current methods for overcoming this problem, such as reducing contact resistances or back gating, tend to increase dark current and suffer slow response times. Here, we realize the avalanche effect in a 2D material-based photodetector and show that avalanche multiplication can greatly enhance the device response of an ultrathin InSe-based photodetector. This is achieved by exploiting the large Schottky barrier formed between InSe and Al electrodes, enabling the application of a large bias voltage. Plasmonic enhancement of the photosensitivity, achieved by patterning arrays of Al nanodisks onto the InSe layer, further improves device efficiency. With an external quantum efficiency approaching 866%, a dark current in the picoamp range, and a fast response time of 87 ?s, this atomic layer device exhibits multiple significant advances in overall performance for this class of devices.

REPORT DOCUMENTATION PAGE (SF298)
(Continuation Sheet)

Continuation for Block 13

ARO Report Number 59735.119-MS-MUR
An Atomically Layered InSe Avalanche Photode...

Block 13: Supplementary Note

Approved for public release; distribution is unlimited.

NANO LETTERS

Letter

pubs.acs.org/NanoLett

An Atomically Layered InSe Avalanche Photodetector

Sidong Lei,[†,▽] Fangfang Wen,[‡,§,▽] Liehui Ge,[†] Sina Najmaei,[†] Antony George,[†] Yongji Gong,[†] Weilu Gao,[⊥] Zehua Jin,[†] Bo Li,[†] Jun Lou,[†] Junichiro Kono,[†,∥,⊥] Robert Vajtai,[†] Pulickel Ajayan,*[,†,‡] and Naomi J. Halas*[,‡,§,∥,⊥]

[†]Department of Materials Science and NanoEngineering, Rice University, Houston, Texas 77005, United States

[‡]Department of Chemistry, Rice University, Houston, Texas 77005, United States

[§]Laboratory for Nanophotonics, Rice University, Houston, Texas 77005, United States

[∥]Department of Electrical and Computer Engineering, Rice University, Houston, Texas 77005, United States

[⊥]Department of Physics and Astronomy, Rice University, Houston, Texas 77005, United States

Supporting Information

ABSTRACT: Atomically thin photodetectors based on 2D materials have attracted great interest due to their potential as highly energy-efficient integrated devices. However, photoinduced carrier generation in these media is relatively poor due to low optical absorption, limiting device performance. Current methods for overcoming this problem, such as reducing contact resistances or back gating, tend to increase dark current and suffer slow response times. Here, we realize the avalanche effect in a 2D material-based photodetector and show that avalanche multiplication can greatly enhance the device response of an ultrathin InSe-based photodetector. This is achieved by exploiting the large Schottky barrier formed between InSe and Al electrodes, enabling the application of a large bias voltage. Plasmonic enhancement of the photosensitivity, achieved by patterning arrays of Al nanodisks onto the InSe layer, further improves device efficiency. With an external quantum efficiency approaching 866%, a dark current in the picoamp range, and a fast response time of 87 μs, this atomic layer device exhibits multiple significant advances in overall performance for this class of devices.

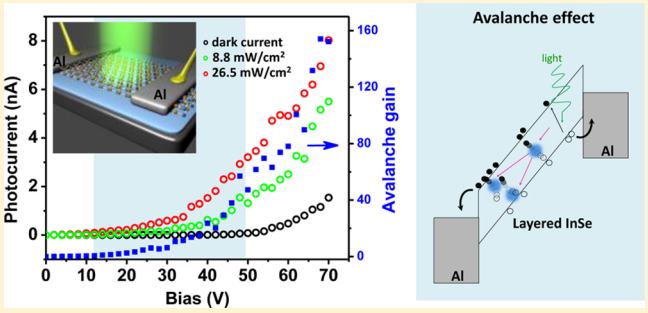

KEYWORDS: *InSe, 2D photodetector, avalanche effect, impact ionization*

Atomically thin two-dimensional (2D) materials have attracted great attention during the past decade and are expected to change the geometries of electronic,[1,2] photonic, and optoelectronic[3] devices. 2D materials show great potential in compact, ultrathin, even flexible photodetector and photovoltaic devices,[4−7] providing a new strategy for integrated electronics with inherently low energy consumption. Thus far, three groups of 2D materials have attracted the most interest for photodetection applications: graphene,[8−12] transition metal dichalcogenides (e.g., MoS_2[13,14] and WS_2[15]), and III−VI layered semiconductors (e.g., GaS,[16] GaSe,[17,18] InSe,[19] GaTe,[20] and In_2Se_3[21]). An inherent limitation of these materials, however, is weak photocurrent generation due to their limited optical absorption cross sections, so their overall photosensitivity is rather low. This can be enhanced by improving the quality of contacts to reduce contact resistance[13] or by back-gating the device.[13,20] These approaches may improve electron injection into the material from the metal contact and also improve the conductivity of the material in a device geometry. The quantum efficiency (QE) of these devices can exceed 100%,[13,18,20,22,23] however, these high efficiencies are also typically accompanied by high levels of dark current (e.g., GaSe ∼80 nA,[18] MoS_2 several microamperes,[13] GaTe ∼0.3 μA,[20] In_2Se_3 ∼200 pA[22]), resulting in poor signal-to-noise ratios (S/N, signal power divided by variance induced by noise). Furthermore, most of the device geometries that have been reported exhibit long response times, which limit potential applications.

For photodetection, responsivity and external quantum efficiency are not the only device characteristics to be considered because an external amplification circuit can always be used to improve them. However, S/N and response time cannot be substantially improved by further signal processing. These limitations become even more problematic when background noise affects the measurement or the signal level for measurement is low, for example, when photodetectors are used in spectroscopic applications. A fast response is crucial for their applications in high-speed image capturing, sensing, telecommunications, and so forth. As a result, low dark currents, a high S/N, and short response times are as important

Received: January 3, 2015
Revised: March 11, 2015
Published: March 30, 2015

DOI: 10.1021/acs.nanolett.5b00016
Nano Lett. 2015, 15, 3048−3055

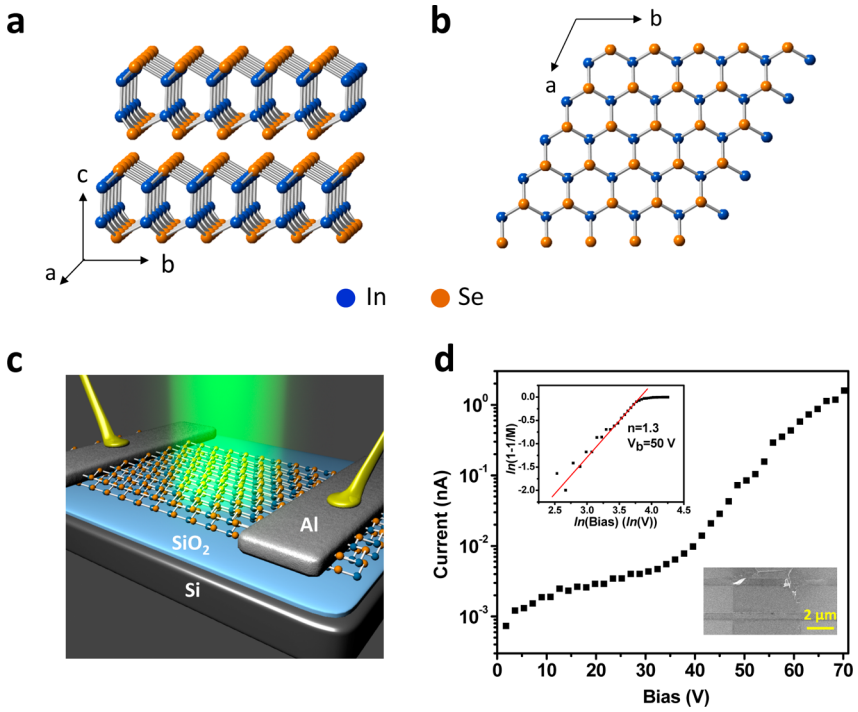

Figure 1. Crystal structure of InSe, schematic representation, and breakdown analysis of the layered InSe avalanche photodetector. (a) Side view and (b) top view of the InSe crystal structure. The spacing between two adjacent layers is 8.4 Å, and the lattice constant along the *a* axis is 4 Å. Each layer has a hexagonal structure with D_{3h} symmetry. (c) Schematic of atomically layered InSe avalanche photodetector. InSe flake was exfoliated and positioned on a silicon substrate coated with a 285 nm thermal oxide layer. Aluminum electrodes were patterned on top of the InSe flake using electron beam lithography. The thickness of the electrodes is 35 nm. This configuration forms two back-to-back Al−InSe Schottky diodes. A 543 nm wavelength He/Ne laser was focused onto the device to excite carriers. The photocurrent was collected via applying a bias voltage across the Schottky contacts. (d) Dark current $I-V$ curve of a layered InSe avalanche photodetector (right bottom inset) showing distinct current responses at different applied biases. The bias voltage is applied all the way up to 70 V for the studied device here. Analysis on the avalanche breakdown is shown in the left upper inset. For the avalanche effect in ionization, the gain (M) and the bias voltage (V) satisfy $M = (1/(1 - (V/V_b)^n))$, where V_b is the critical voltage and n is the index relevant to ionization scattering cross section. By fitting current response with a transformed linear relationship $(1 - (1/M)) = n \times (\ln(V) - \ln(V_b))$, as indicated by the red line in the inset, V_b and n values can be retrieved, where V_b is determined to be 50 V and n is 1.3.

as responsivity. The challenge is how to increase photoresponsivity without compromising other aspects of device performance and how to most effectively generate and use as many photocarriers as possible in a device.

Here, we demonstrate a 2D material-based photodetector, based on atomically layered InSe, that utilizes the avalanche effect to improve photoresponsivity, lower dark currents, and reduce device response times. The avalanche effect is achieved by creating large Schottky barriers between the 2D material and the aluminum electrodes, so that a large electrical field can be applied across the InSe sample to trigger the avalanche effect before reverse bias breakdown. Also, due to the existence of a reverse-biased Schottky barrier, the dark current is dramatically reduced. We achieve a 334% external quantum efficiency with an avalanche gain of 47, a low picoamp level dark current, and a response time of 60 μs, all advancing the overall performance of the 2D photodetector. When a larger bias is applied, the quantum efficiency is further increased to 1110% with an avalanche gain of 152. Aluminum plasmonic nanostructures are fabricated onto the active face of the device to increase photocurrent generation even further through hot electron injection and local field enhancement. The quantum efficiency is increased by 800%: a dramatic improvement in device performance.

The avalanche effect occurs when a large external electrical field is applied to a semiconductor to accelerate the charge carriers to sufficiently high energy that they can generate additional electron−hole pairs through collisional ionization. If photogenerated charge carriers are accelerated, the photoresponse can be strongly amplified by this multiplication process. Because photocarriers alone provide the major current source to trigger the avalanche effect, when no additional noise source is introduced, for example, by an external amplifier, S/N values can in principle be extremely high under standard device operating conditions.

Our InSe-based atomically layered avalanche photodetector (APD) is fabricated with aluminum electrodes, forming large Schottky barriers. The large Schottky barriers between Al and InSe allow us to apply a large electrical field across the device (60 kV/cm), to induce the avalanche effect. As previous reported,[19] InSe is a good candidate material for photodetectors, having a layered structure (Figure 1a, b), with an in-plane lattice constant of 0.40 nm and an interlayer spacing of 0.83 nm. InSe atomic layers were exfoliated from a bulk InSe crystal using Scotch tape and transferred onto SiO_2/Si substrates (SiO_2 layer is 285 nm). Electrodes were patterned using e-beam lithography, followed by e-beam deposition of 35 nm Al and lift-off. The width of the Al electrodes is 500 nm, and the channel spacing is 2 μm. The schematic of the device configuration is shown in Figure 1c and the SEM image of the device under test is shown in Figure 1d (inset). The APD device consists of two Schottky junctions sitting back to back.

DOI: 10.1021/acs.nanolett.5b00016
Nano Lett. 2015, 15, 3048−3055

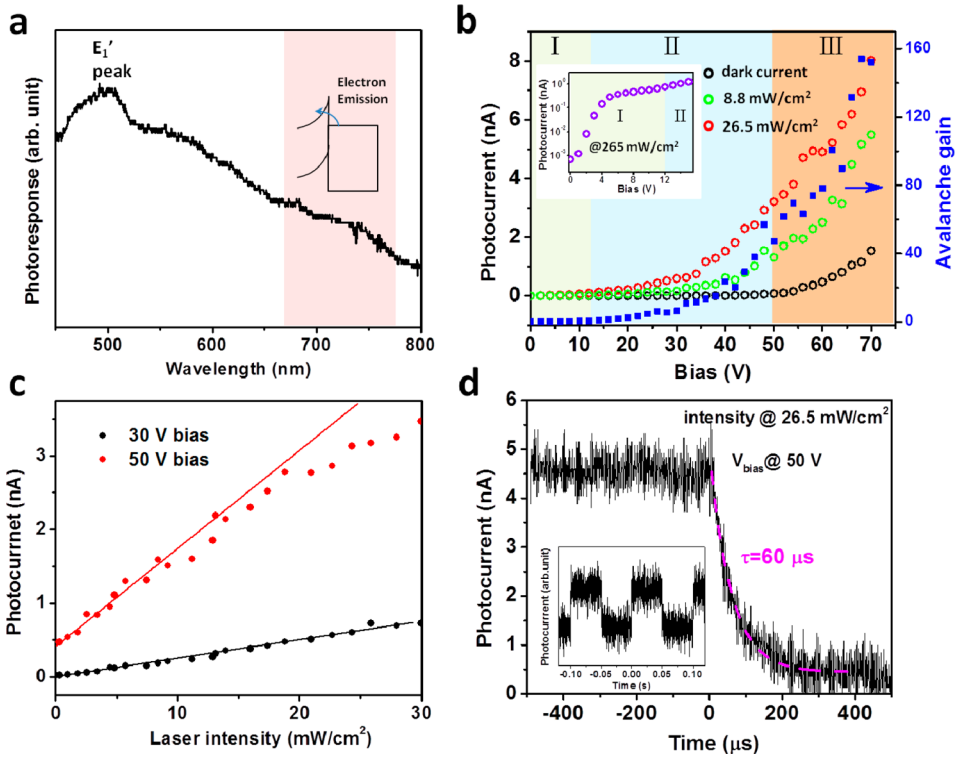

Figure 2. Photoconductivity characteristics of the layered InSe avalanche photodetector. (a) Photocurrent spectrum of an atomically layered InSe flake. The photocurrent peak at ~510 nm corresponds to the E_1' interband transition in layered InSe. (b) Photocurrent response of layered InSe avalanche photodetector under different illumination intensities. Photocurrent curve shows a nonlinear dependence on the bias voltage. The photocurrent response can be divided into three regions. Below 12 V bias (region I), as it is shown clearly in the inset, photocurrent increases quickly with the applied bias and starts to saturate at 12 V. Beyond 12 V (region II), a dramatic increase of the photocurrent emerges, and the current increases rapidly with a bias all the way to ~50 V. Avalanche effect takes place in this region, and the dark current remains relatively small, varying from few picoamperes to <100 pA. When the bias voltage is greater than ~50 V (region III), a sudden increase in dark current can be seen due to the reverse bias breakdown. As a consequence, the photocurrent increases greatly as well. (c) Power-dependent photoresponse of the layered InSe avalanche photodetector at a 30 and 50 V biases. The device shows a linear response in the power range from 0 to 30 mW/cm^2 at a 30 V bias. If the bias is increased to 50 V, photocurrent response starts to deviate from linear increase trend. (d) Time-resolved photocurrent response shows a decay time constant of 60 μs of the photodetector under a 26.5 mW/cm^2 illumination intensity and a 50 V bias voltage.

In the absence of illumination, there is always one reverse-biased Schottky junction, which minimizes the dark current. When illuminated, electron−hole pairs are generated and separated by an external field applied to the device. In this case, electrons can pass through the forward-biased junction and holes can pass through the reverse-biased junction. The charge carriers flow through the external circuit to recombine and generate the photocurrent. The high Schottky barriers minimize the dark current and enable the application of large biases across the device to trigger avalanche multiplication before the breakdown of Schottky junction. Without this large Schottky barrier, the application of a large enough bias to achieve avalanche multiplication would not be possible.

The dark current of the device is shown in Figure 1d. The dark current increases gradually with bias voltage, saturates at ~12 V, then begins to rise dramatically when the bias is further increased. When the bias is below 12 V, the reverse-biased Schottky barrier allows a small current to flow, which also saturates at 12 V. The current at 12 V is defined as the saturation current I_{sat} of the Schottky barrier, the maximum current that can pass through the reverse-biased Schottky barrier without illumination or any kind of breakdown. When the bias voltage is increased to values above 12 V, the charge carriers passing through the InSe−Al junction begin to be accelerated to a high energy which can generate more charge carriers by ionization collisions. This current increase is the onset of avalanche behavior. The charge carrier multiplication M is defined as

$$M = \frac{I}{I_{sat}} \tag{1}$$

where I_{sat} is the current at 12 V and I is the current above 12 V.

To further confirm the avalanche effect and determine its characteristics in this device, we perform a more detailed analysis of the device behavior. According to the theoretical model of the avalanche effect, when this behavior occurs, charge carrier multiplication M follows this behavior[24]

$$M = \frac{1}{1 - \left(\frac{V}{V_b}\right)^n} \tag{2}$$

where n is the index corresponding to the ionization rate and V_b is the critical voltage. (V_b here is only a fitting parameter of eq 2, and does not indicate that the avalanche effect takes place at this value. Instead, the avalanche effect occurs at far lower voltages.) Equation 2 can be rewritten in a linear form

$$\ln\left(1 - \frac{1}{M}\right) = n \times (\ln(V) - \ln(V_b)) \tag{3}$$

DOI: 10.1021/acs.nanolett.5b00016
Nano Lett. 2015, 15, 3048−3055

The current multiplication ($M = I/I_{sat}$) is plotted using eq 3 (Figure 1d, inset), which clearly matches the theoretical model for applied voltages below 50 V. The linear relationship between $\ln(1 - 1/M)$ and $\ln(V)$ clearly substantiates that the avalanche effect takes place within the device for an applied voltage above 12 V. This corresponds to an electrical field larger than 60 kV/cm, which we will refer to as the threshold field in our analysis. The threshold field is found to be very consistent for all the devices. (See Supporting Information Figure S1 for more electrical characterization data gathered on several different devices.) By fitting the inset figure with eq 3, n is determined to be 1.3, and V_b is 50 V. When the bias voltage is increased above 50 V, the dark current increases even more rapidly, which we attribute to reverse bias breakdown. The avalanche effect still continues when the bias voltage is greater than 50 V, but it is accompanied by other effects.

The dark current behavior suggests that there are three regimes for this device. For small bias voltages (<12 V), no avalanche effect occurs. Between 12 and 50 V, avalanche behavior is triggered and charge carrier multiplication occurs. Above 50 V, reverse bias breakdown happens and the dark current increases dramatically. Therefore, the optimal device behavior occurs for a range of applied bias voltages between 12 to 50 V.

The photocurrent spectrum of layered InSe is shown in Figure 2a, which clearly exhibits a peak at 510 nm, corresponding to the E_1' transition in few-layered InSe.[19] An SEM image of the device is shown in Figure 1d (lower inset). We observe that the photocurrent response is also extended to red and near-infrared wavelengths when the device is patterned with Al electrodes, as shown in the shaded area in Figure 2a: the photoresponse is stronger in the 650−750 nm range in comparison with a previously reported study using gold electrodes.[19] (In the following discussion of Al plasmonic enhanced devices, this phenomenon becomes more prominent.) This effect is attributed to photoexcited electron emission over the Schottky barrier from the Fermi energy of the metal. The Schottky contact between the Al metal electrode and InSe can contribute to the photoresponse of the device: from the device behavior, the Schottky barrier height is determined to be nominally 1.54 eV (Supporting Information Figure S2). As a comparison, we also fabricated an InSe photodetector with Ti/Au electrodes. Because of the lower Schottky barrier height, no avalanche effect was observed, and the device showed a longer response time (refer to Supporting Information Figure 3S for details). The photoresponse of the device is shown in Figure 2b, which was measured in the dark and under illumination by a 543 nm He/Ne laser with intensities of 8.8 mW/cm^2 (green circles) and 26.5 mW/cm^2 (red circles). We find that the dark current (black circles) does not increase significantly as a function of bias voltage until 50 V; this is due to the presence of the reverse-biased Schottky junction that effectively minimizes the dark current to the picoamp level. When the bias is beyond 50 V, the dark current increases dramatically to the nanoamp level as a result of the reverse bias breakdown. Operation of the APD in this voltage range (above 50 V in our case) is not recommended because the large dark current would greatly reduce the S/N ratio. Also under large bias voltages the current changes significantly with small changes in bias voltage (i.e., the dark current in this region is not stable and the device generates substantial noise). Just as with the dark current, the photocurrent also shows a distinct response under different bias voltages: Below 5 V, the photocurrent increases quickly with applied bias, then starts to saturate until 12 V (Figure 2b, inset); then increases dramatically between 12 and 50 V (region II) due to the avalanche effect.[25] At a 50 V bias and 8.8 mW/cm^2 illumination intensity, the quantum efficiency is determined to be 344%, (refer to Supporting Information for the detailed calculation) corresponding to an avalanche gain of 47. Above 50 V bias (region III), the quantum efficiency can reach 1110% with a gain of 152. The avalanche gain saturates when we increase the illumination intensity further to 26.5 mW/cm^2, when the quantum efficiency drops to 290% with an avalanche gain of 24. We also studied the photocurrent response as a function of illumination intensity at different biases (Figure 2c). At a 30 V bias, the photoresponse is linear with illumination intensity. The linear dynamic range (= 20 log (I_{ph}/I_{dk})) is larger than 103 dB. However, at a 50 V bias, the photoresponse starts to saturate after 20 mW/cm^2 illumination, and the linear dynamic range is reduced to ∼70 dB. These results show that our 2D layered APD is more efficient in detecting low-level signals, a typical feature of avalanche photodetectors.

Besides its high gain, a faster response time is another advantage of our APD over other 2D photodetectors that use other multiplication methods, such as back gating. To date, numerous photodetectors have exploited back gating to improve quantum efficiencies, largely attributed to the presence of high densities of trap states to recombine the electrons and holes and thus increase the internal gain.[26] Although the QE of the device is greatly increased, the response time of the device is largely compromised by that approach to the level of milliseconds and even seconds.[13,18] We performed time-resolved measurements on our APD (Figure 2d), obtaining a response time of 60 μs. This is faster than most reported 2D-based photodetectors.[13,18] To make a direct comparison, we also applied a gate voltage to our device. By applying a 10 V bias voltage and a 40 V gate voltage, we amplified the photoresponse signal to the same level as with the InSe APD without back gating. We found that the response time with back gating is significantly increased to 4.2 ms, a response about 2 orders of magnitude longer than the InSe APD without back gating due to creation of trapping states (refer to Supporting Information Figure S4 for a more detailed discussion). Another significant advantage of InSe APD is the low dark current. Back gating also increased the dark current to the level of hundreds of picoamps to nanoamps, more than an order of magnitude larger than our InSe APD without back gating.

With the measured response speed and dark current, it is possible to calculate the S/N of the device. The dark current determines the noise level, which can be expressed as

$$\sigma^2 = 2e \times I_d \times \mathrm{BW} \times M^2$$

and the signal-to-noise ratio is expressed as $(S/N) = ((I_{ph}^2)/(\sigma^2))$, where e is charge of electron, I_d is dark current, BW is bandwidth (because the response time is 60 μs, it is reasonable to set it to 16 kHz), and M is the avalanche photodetector gain. Under a 26.5 mW/cm^2 illumination, the S/N is 60 dB at 30 V bias, and 46 dB at 50 V bias. (Refer to Supporting Information for the detailed calculation.) If the bias is further increased to 70 V, in the reverse bias breakdown voltage region, the S/N drops to 35 dB as a result of the dramatically larger dark current and a higher gain. (Refer to Supporting Information Figure S5 for a more detailed S/N discussion.) In contrast, the gated device with a similar photoresponse level gives a S/N of 27 dB.

DOI: 10.1021/acs.nanolett.5b00016
Nano Lett. 2015, 15, 3048−3055

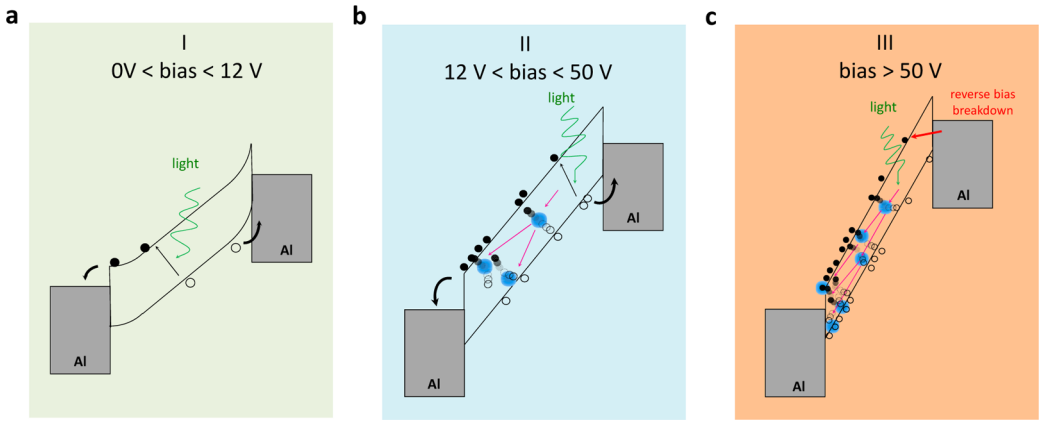

Figure 3. Working principle of the layered InSe avalanche photodetector at the different applied biases shown in Figure 2b. When the voltage is applied to the Al electrodes, one Schottky diode is forward-biased (left), whereas the other is reverse-biased (right). (a) In region I with a bias lower than 12 V, the forward-biased Schottky barrier is compensated by the electrical field applied by the bias voltage so that electrons can pass through the barrier freely and be collected by the electrode. Meanwhile, photogenerated holes are driven to the reverse-biased electrode. In this case, photocurrent is generated. (b) When the bias is increased beyond 12 V (region II, from 12 to 50 V), the external electrical field exerted on the InSe layers is so large that the photoexcited electrons are accelerated to a high energy. This will generate additional electron−hole pairs by carrier multiplication, that is, the avalanche effect. (c) When the bias is larger than 50 V (region III), the reverse-biased Schottky barrier becomes thinner, where the possibility of quantum tunneling increases dramatically.

On the basis of the above discussion, a clearer physical picture can be established for each of the operating voltage ranges (Figure 3). When a small bias (<12 V) is applied to the device (Figure 3a, region I), the photocurrent is very low. In this region, the external field is not strong enough for carriers to the trigger avalanche effect, in other words, the InSe APD operates just as an ordinary photodetector in this region. As the external field increases, the rate of electron−hole pair separation and transport become faster and the QE increases until all the photogenerated charge carriers contribute to photoconductivity before recombination, and consequently, saturation occurs.

When the electric field is increased further, carrier multiplication due to the avalanche effect can be observed (Figure 3b, region II). Photocurrent shows a rapid increase with the applied bias. The higher the electrical field, the more carrier multiplication occurs and higher gain values can be achieved. When the electrical field reaches the maximum for the device, the reverse-biased Schottky barrier undergoes breakdown (Figure 3c, region III). If the bias is increased beyond this point (~50 V or higher), both dark current and photocurrent increase dramatically. However, S/N suffers due to the high dark current. The best operating range for this device is between 30 and 50 V.

All these effects are due to the Schottky barrier that is formed between the InSe and Al, which allows us to minimize the dark current and realize avalanche-based carrier multiplication. In other words, we can utilize the photoelectrons more effectively, but the number of photogenerated carriers is not increased. The device performance can be improved even further by generating more photoelectrons. One limitation is the low light absorption due to the limited thickness of the 2D layer. Plasmonic nanostructures patterned onto the active InSe face of the device can be used to enhance light absorption.[27] Recent work has demonstrated that Al is an outstanding plasmonic material in the UV and visible regions of the spectrum,[28] which corresponds well to the photoresponsivity spectrum of layered InSe.

Plasmonic Al disk nanoantennas were fabricated onto our device for absorption enhancement. A schematic of the patterned device is shown in Figure 4a, and the SEM image of the fabricated device is shown in Figure 4b. The Al electrodes and nanodisks were patterned using e-beam lithography, followed by e-beam evaporation of Al and lift off. The aluminum disks are 150 nm in diameter with a thickness of 35 nm and a center-to-center distance of 450 nm. The scattering spectrum of the Al nanodisk array (green dashed curve) and the photoresponse spectra of InSe with (red curve) and without the presence of the Al nanodisks (blue curve) are shown in Figure 4c. The scattering peak of Al nanodisks with these dimensions overlaps with the peak of the photoresponse spectrum of layered InSe (~510 nm), and the photoresponse in this wavelength region is enhanced. In addition, the device photoresponse in the 650 to 750 nm range is also significantly enhanced by the presence of the nanodisks. This can be attributed to electron emission from the Fermi level of the Al nanodisks into InSe, which has the same origin as the electron emission process at the electrodes. The $I-V$ curve of the InSe APD with patterned Al nanodisks is shown in Figure 4d, where we see that the photocurrent is significantly enhanced by the plasmonic nanodisk arrays. With a 30 V bias and 44 mW/cm^2 543 nm incident laser light, the quantum efficiency is increased from 108% (without Al disks) to 866% (with Al disks). The device response shows a linear dependence on incident light intensity at low applied bias (Figure 4e). However, with a 30 V bias, the photocurrent begins to fluctuate with illumination intensity. In this case, the plasmonic enhancement and avalanche effect work together and generate a substantially large photocurrent, on the order of tens of nA, making the APD extremely sensitive to illumination. Plasmonic enhancement also induces a small local heating effect that increases the thermal noise. A further increase in bias voltage would elevate the current to the level where device failure occurs. The plasmonic enhancement allows higher quantum efficiency at a smaller avalanche gain and a larger linear response range. The linearity is maintained up to 90 μW/cm^2, and its dynamic range is improved to 90 dB (Figure 4e).

DOI: 10.1021/acs.nanolett.5b00016
Nano Lett. 2015, 15, 3048−3055

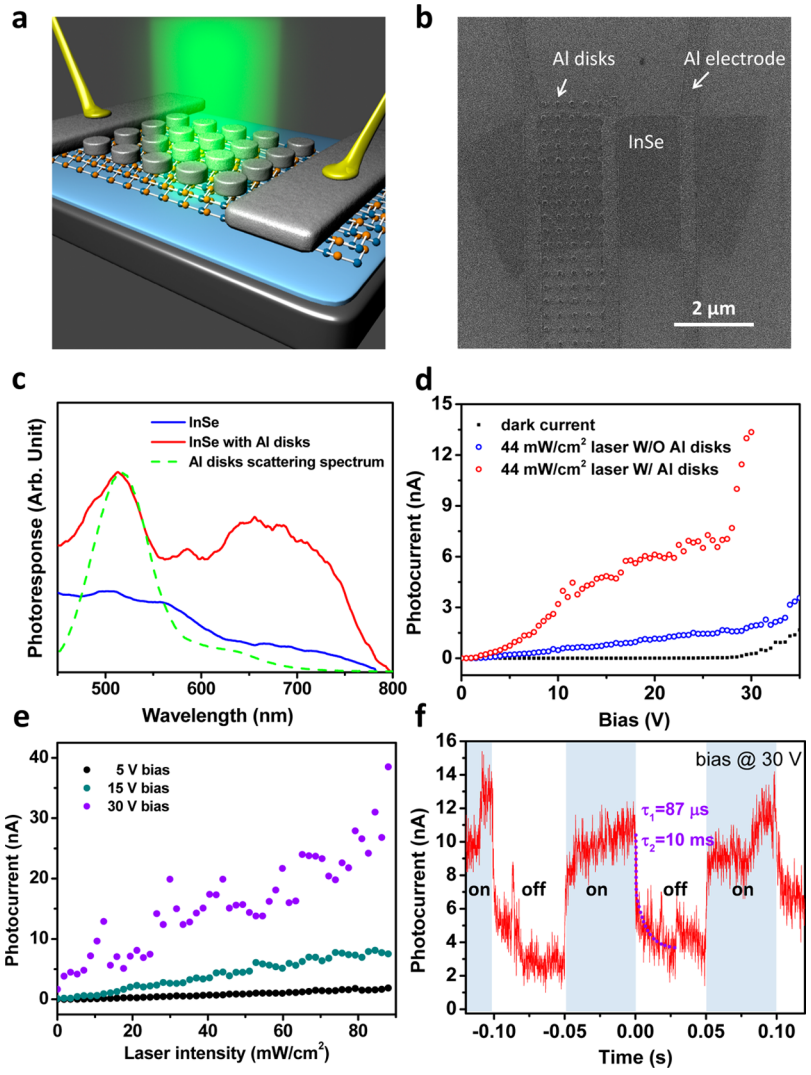

Figure 4. Al nanodisk plasmon-enhanced InSe avalanche photodetector. (a) Schematic of InSe avalanche photodetector patterned with an array of Al nanodisks. (b) Scanning electron microscope images of the InSe device showing regions with and without Al nanodisks. The diameter of Al disks is ∼150 nm and the particles center-to-center distance is 450 nm. Three devices were fabricated simultaneously on the same InSe flake: the one on the left is patterned with Al nanodisks while the two devices one the right are without Al nanodisks. (c) Photocurrent spectra of InSe (blue), InSe decorated with Al nanodisks (red), and the dark-field scattering spectrum of the Al nanodisk arrays (green). The Al nanodisk arrays were designed to be resonant with E_1' transition in InSe flake (∼510 nm). (d) Photocurrent response of InSe device with (red hollow circle) and without (blue hollow circle) Al nanodisks at different laser intensities. The solid black square is the measured dark current. A substantial photocurrent enhancement can be observed for the device decorated with the Al nanodisks. (e) Photoresponse of the device patterned with an Al nanodisks array as a function of laser illumination intensity at 5, 15, and 30 V bias voltages. (f) Time response of the Al plasmon-enhanced InSe avalanche photodetector where two time constants, t_1 = 87 μs and t_2 = 10 ms, can be observed.

Several processes may contribute to the quantum efficiency. First, the Al plasmonic nanodisks provide a local electromagnetic field enhancement that can contribute to carrier generation in the InSe.[27,29] Second, hot electrons generated by the decay of the surface plasmons of the Al nanodisks can provide additional photogenerated carriers, provided that the hot electrons have sufficient energy to cross the Al−InSe Schottky barrier.[30,31] Third, electrons emitted over the Schottky barriers (in the range of 650 to 750 nm) are accelerated to a high kinetic energy, further contributing to the avalanche process. However, resonantly excited Al nanodisks also induce a small local heating effect,[32] which can shorten the excited carrier lifetime.

The time-resolved photoresponse of the Al nanodisk patterned device is shown in Figure 4f. The decay behavior differs significantly from the device without Al nanodisks, having two distinct time constants (t_0 and t_1 from equation $I = I_0e^{-(t/t_0)} + I_1e^{-(t/t_1)}$). One time constant is 87 μs, which is close to the photoresponse of the InSe avalanche photodetector without plasmonic Al nanodisks (shown in Figure 2). A second, longer time constant of 10 ms is also present. There are two possible mechanisms that may contribute to this long time constant. One could be capacitive charging due to hot electron injection from the electrically isolated Al nanodisks into the InSe: charge neutralization of the nanodisks necessitates carrier diffusion back into the structures. Another could be thermal effects due to local heating of device by illumination of the Al nanodisks.

In summary, we have observed the avalanche effect in 2D semiconductors for the first time. We have successfully demonstrated an atomically thin InSe avalanche photodetector using a double Schottky barrier device design that enhances

DOI: 10.1021/acs.nanolett.5b00016
Nano Lett. 2015, 15, 3048−3055

external quantum efficiency while maintaining a low dark current and a fast response time. Our avalanche photodetector improves the external quantum efficiency to 344% with an avalanche multiplication of 47X and a dark current below the tens of picoamps range, and a response time of 60 μs. The performance of the device has been further improved through the introduction of plasmonic Al nanodisks for enhancing photocurrent generation. This combination of the avalanche effect and plasmonic enhancement collectively improves the external quantum efficiency to 866%. Similar strategies can also be applied quite generally to enhance the overall performance of photodetectors fabricated using other 2D materials.

Methods. *Device Fabrication.* InSe atomic layers were exfoliated from a bulk InSe crystal using Scotch tape and transferred onto a Si substrate coated with 285 nm SiO_2. Al electrodes and Al nanodisks were patterned by e-beam lithography using a scanning electron microscope (FEI QUANTA 650), followed by e-beam deposition of 35 nm Al in an high vacuum chamber ($4e^{-7}$ Torr). Lift off was performed at room temperature using acetone, followed by a rinse with isopropyl alcohol and nitrogen drying. The scattering spectrum of Al disk array was measured by a dark-field microspectroscope. The white light source was focused to the sample by a 50× dark-field objective with a numerical aperture of 0.55, and the scattered signal was directed into the spectrograph (Princeton instruments Acton 2156i) and CCD (Pixis 400 BR). The spectrum was obtained by dividing the collected signals with the white light spectrum after background subtraction.

Photoconductivity Measurement. Photoconductivity measurements were performed on a home-built probe-station with a 1-in. fused silica optical window for sample illumination and a vacuum pressure of 10^{-5} Torr. A 543 nm He/Ne laser was focused and injected into an acoustic optical modulator (AOM) for laser intensity stabilization, controlling, and modulation (for light pulse generation in time-resolved measurement). The turn-on and turn-off time of the AOM was optimized to be nominally 200 ns. After passing through the AOM, the laser output was directed onto the optical window and focused onto the sample placed inside the vacuum probe-station, with a spot size of 0.6 mm in diameter for a uniform illumination. The $I-V$ curves under different illumination intensities were measured with a Keithley 2634B dual-channel source-meter unit (SMU) connected to the probe-station with a triaxial cable for low-noise measurement. Time-resolved measurement data was amplified by a Stanford Research Systems (SR570) low-noise current preamplifier with a bandwidth of 200 kHz, and recorded by a 10 MHz bandwidth Teletronix oscilloscope. For the photocurrent spectrum measurement, the device was illuminated at normal incidence by a xenon lamp coupled with a Newport Corner Stone monochromator for frequency selectivity. At each frequency, photocurrent was amplified by a SRS low-noise current preamplifier with a bandwidth set at 10 kHz, and recorded by the oscilloscope. The bias voltage was fixed at 17 V for photocurrent spectrum measurement.

■ ASSOCIATED CONTENT

Supporting Information

More avalanche $I-V$ curve fitting, Schottky barrier estimation, the performance of InSe photodetector with Ti/Au electrodes, and the performance of InSe photodetector with gating. This material is available free of charge via the Internet at http://pubs.acs.org.

■ AUTHOR INFORMATION

Corresponding Authors

*E-mail: ajayan@rice.edu.
*E-mail: halas@rice.edu.

Author Contributions

[▽]Sidong Lei and Fangfang Wen contributed equally to this work.

Notes

The authors declare no competing financial interest.

■ ACKNOWLEDGMENTS

The authors thank Bob Zheng, Ali Sobhani, Dr. Aditya Mohite, and Dr. Gautam Gupta for discussions. This work was supported by the Robert A. Welch Foundation under Grants C-1220, the National Security Science and Engineering Faculty Fellowship (NSSEFF) N00244-09-1-0067, and the Office of Naval Research N00014-10-1-0989. This work was also supported by the MURI ARO program W911NF-11-1-0362, by FAME, one of six centers of STARnet, a Semiconductor Research Corporation program sponsored by MARCO and DARPA and by Netherlands organization for scientific research (NWO) under the framework of Rubicon program (project number 680-50-1205). Sina Najmaei and Jun Lou were supported by Welch grant C-1716. Jun Lou and Pulickel Ajayan were also supported by NSF ECCS 1327093.

■ REFERENCES

(1) Schwierz, F. *Nat. Nanotechnol.* **2011**, *6*, 135−136.
(2) Li, L.; Yu, Y.; Ye, G. J.; Ge, Q.; Ou, X.; et al. *Nat. Nanotechnol.* **2014**, *9*, 372−377.
(3) Britnell, L.; Ribeiro, R. M.; Eckmann, A.; Jalil, R.; Belle, B. D.; et al. *Science* **2013**, *340*, 1311−1314.
(4) Bernardi, M.; Palummo, M.; Grossman, J. C. *Nano Lett.* **2013**, *13*, 3664−3670.
(5) Ross, J. S.; Klement, P.; Jones, A. M.; Ghimire, N. J.; Yan, J.; et al. *Nat. Nanotechnol.* **2014**, *9*, 268−272.
(6) Pospischil, A.; Furchi, M. M.; Mueller, T. *Nat. Nanotechnol.* **2014**, *9*, 257−261.
(7) Baugher, B. W.; Churchill, H. O.; Yang, Y.; Jarillo-Herrero, P. *Nat. Nanotechnol.* **2014**, *9*, 262−267.
(8) Bao, Q.; Loh, K. P. *ACS Nano* **2012**, *6*, 3677−3694.
(9) Bonaccorso, F.; Sun, Z.; Hasan, T.; Ferrari, A. C. *Nat. Photonics* **2010**, *4*, 611−622.
(10) Mueller, T.; Xia, F.; Avouris, P. *Nat. Photonics* **2010**, *4*, 297−301.
(11) Xia, F.; Mueller, T.; Lin, Y.-m.; Valdes-Garcia, A.; Avouris, P. *Nat. Nanotechnol.* **2009**, *4*, 839−843.
(12) Furchi, M.; Urich, A.; Pospischil, A.; Lilley, G.; Unterrainer, K.; et al. *Nano Lett.* **2012**, *12*, 2773−2777.
(13) Lopez-Sanchez, O.; Lembke, D.; Kayci, M.; Radenovic, A.; Kis, A. *Nat. Nanotechnol.* **2013**, *8*, 497−501.
(14) Yin, Z.; Li, H.; Jiang, L.; Shi, Y.; Sun, Y.; et al. *ACS Nano* **2012**, *6*, 74−80.
(15) Perea-López, N.; Elías, A. L.; Berkdemir, A.; Castro-Beltran, A.; Gutiérrez, H. R.; et al. *Adv. Funct. Mater.* **2013**, *23*, 5511−5517.
(16) Hu, P.; Wang, L.; Yoon, M.; Zhang, J.; Feng, W.; et al. *Nano Lett.* **2013**, *13*, 1649−1654.
(17) Lei, S.; Ge, L.; Liu, Z.; Najmaei, S.; Shi, G.; et al. *Nano Lett.* **2013**, *13*, 2777−2781.
(18) Hu, P.; Wen, Z.; Wang, L.; Tan, P.; Xiao, K. *ACS Nano* **2012**, *6*, 5988−5994.
(19) Lei, S.; Ge, L.; Najmaei, S.; George, A.; Kappera, R.; et al. *ACS Nano* **2014**, *8*, 1263−1272.
(20) Liu, F.; Shimotani, H.; Shang, H.; Kanagasekaran, T.; Zolyomi, V.; et al. *ACS Nano* **2014**, *8*, 752−760.

DOI: 10.1021/acs.nanolett.5b00016
Nano Lett. 2015, 15, 3048−3055

(21) Lin, M.; Wu, D.; Zhou, Y.; Huang, W.; Jiang, W.; et al. *J. Am. Chem. Soc.* **2013**, *135*, 13274−13277.
(22) Jacobs-Gedrim, R. B.; Shanmugam, M.; Jain, N.; Durcan, C. A.; Murphy, M. T.; et al. *ACS Nano* **2014**, *8*, 514−521.
(23) Tamalampudi, S. R.; Lu, Y. Y.; Kumar, U. R.; Sankar, R.; Liao, C. D.; et al. *Nano Lett.* **2014**, *14*, 2800−2806.
(24) Miller, S. L. *Phys. Rev.* **1957**, *105*, 1246−1249.
(25) Yu, J.; Shan, C. X.; Huang, X. M.; Zhang, X. W.; Wang, S. P.; et al. *J. Phys. D: Appl. Phys.* **2013**, *46*, 305105.
(26) Lei, S.; Wen, F.; Li, B.; Wang, Q.; Huang, Y. *Nano Lett.* **2015**, 259−265 DOI: 10.1021/nl503505f.
(27) Sobhani, A.; Lauchner, A.; Najmaei, S.; Ayala-Orozco, C.; Wen, F. F.; et al. *Appl. Phys. Lett.* **2014**, *104*, 031112.
(28) Knight, M. W.; King, N. S.; Liu, L.; Everitt, H. O.; Nordlander, P.; et al. *ACS Nano* **2014**, *8*, 834−840.
(29) Liu, Y.; Cheng, R.; Liao, L.; Zhou, H.; Bai, J.; et al. *Nat. Commun.* **2011**, *2*, 579.
(30) Sobhani, A.; Knight, M. W.; Wang, Y.; Zheng, B.; King, N. S.; et al. *Nat. Commun.* **2013**, *4*, 1643.
(31) Knight, M. W.; Sobhani, H.; Nordlander, P.; Halas, N. J. *Science* **2011**, *332*, 702−704.
(32) Desiatov, B.; Goykhman, I.; Levy, U. *Nano Lett.* **2014**, *14*, 648−652.

DOI: 10.1021/acs.nanolett.5b00016
Nano Lett. 2015, 15, 3048−3055